Electronic Supplementary Material (ESI) for Physical Chemistry Chemical Physics.

Electronic Supplementary Information: Hydrogen Peroxide Generation and Hydrogen Oxidation Reactions of Vacuum-prepared Ru/Ir(111) Bimetallic Surfaces

Kenta Hayashi,*[a] Keisuke Kusunoki,[a] Takeru Tomimori,[a] Riku Sato,[a] Naoto Todoroki,[a] and Toshimasa Wadayama[a]

Graduate School of Environmental Studies, Tohoku University, Sendai 980-8579, JAPAN

*Corresponding Author E-mail Address: kenta.hayashi.r8@dc.tohoku.ac.jp

A. Low-energy Ion Scattering (LE-IS) Spectrum for cleaned Ir(111)

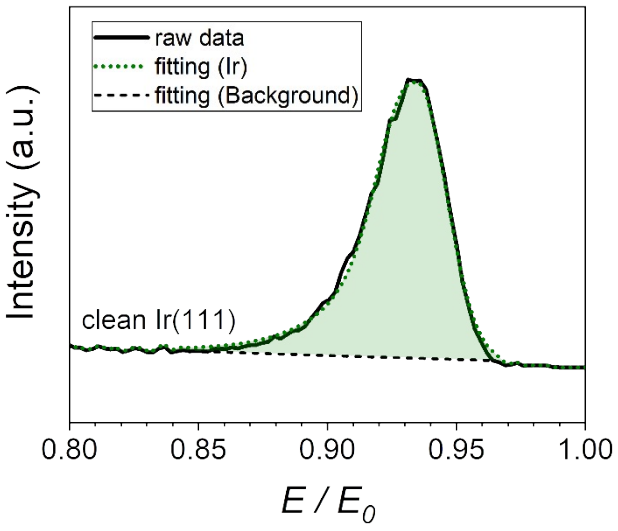

Figure S.1 LE-IS spectrum of clean Ir(111) collected by using the same condition mentioned in the main manuscript

Figure S.1 shows LE-IS spectrum of clean Ir(111). As shown, scattering intensities are asymmetric against (E/E_0) in the present LE-ISS condition.

B. Scanning Tunnelling Microscopy (STM)

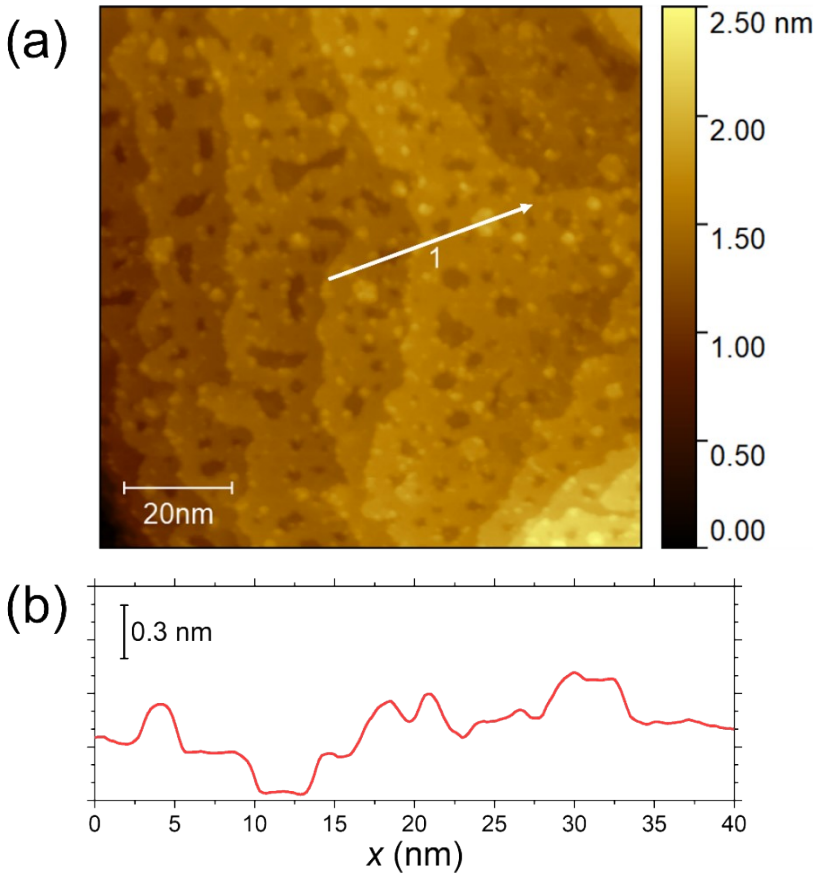

Figure S.2 STM image (a) and line profile (b) for the surface of 773 K-Ru/Ir(111)

Scanning tunnelling microscopy (STM) images were collected for 773 K-Ru/Ir(111) (Figure S.2(a)). Sample preparation and STM observations were conducted in the same vacuum system as that used for XPS and LE-ISS. The Ru deposition for STM observations was conducted at room temperature (ca. 298 K), followed by annealing at 773 K for 30 min. During the STM observations, the substrate temperature was room temperature. Typical tunnel currents and tunnel voltages were 0.1–0.05 nA and 500–2000 mV, respectively. In Figure S.2(a), the terraces with a width of approximately 20 nm corresponds to the (111) plane of the Ir(111) substrate.

Figure S.2(b) shows height fluctuations of corresponding a white arrow on the image of (a). The profile indicates that pit-like structures and cluster-like structures, which is mono-atomic-height (less than 0.3 nm) and nano-meter-width, are generated probably through the inter-diffusion of APD Ru and substrate Ir atoms at the substrate temperature of 773 K. However, no evident agglomerated structures were observed on the image, confirming that the 773 K-Ru/Ir(111) is atomically flat. Considering the Ir-Ru phase diagram shows the large solubility of Ru in FCC Ir (ca. 40 at.%),[1] the prepared surfaces are likely to be the homogeneous Ir-Ru alloy solid solution.

C. H_2O_2 Generation Behaviour of Ru(0001)

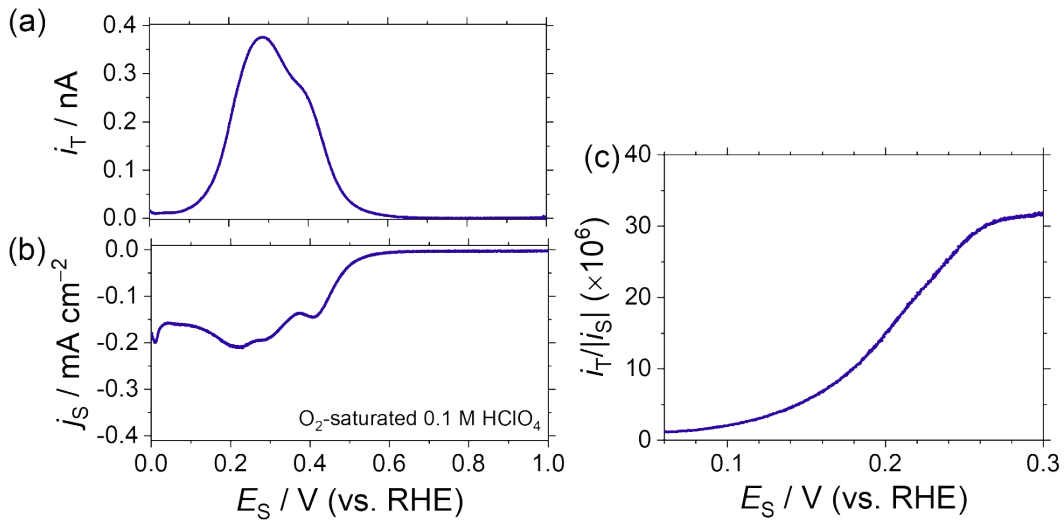

Figure S.3 (a) Pt UME tip current for H_2O_2 detection (i_T), (b) substrate current density (j_S), and (c) tip current normalized by substrate current ($i_T/|i_S|$) for clean Ru(0001) recorded by the SG/TC mode of SECM in O_2-saturated 0.1 M $HClO_4$

Figure S.3 shows H_2O_2 generation for vacuum-cleaned Ru(0001) evaluated by the SG/TC mode of SECM. The measurement procedure is described in the experimental section in the main text. Pt UME tip current (i_T; a) markedly increases between ca. 0.6 V and 0.1 V (Figure S.3(a)). Specifically, i_T peaks around 0.3 V with an accompanying shoulder at approximately 0.4 V. The i_T response indicates the generation of H_2O_2 in the corresponding potential region. As shown in (b), in contrast, substrate current density, (j_S) which mainly originated from oxygen reduction, begins to increase below 0.6 V during the negative going potential scan. Complex responses of j_s (peaked at ca. 0.4, 0.3, and 0.2 V) suggest the superimposition of several electrochemical reduction processes during the measurement, although the detailed electrochemical steps proceeding on Ru(0001) remain unresolved.

D. Cyclic Voltammograms (CVs) of *x* K-Ru/Ir(111)

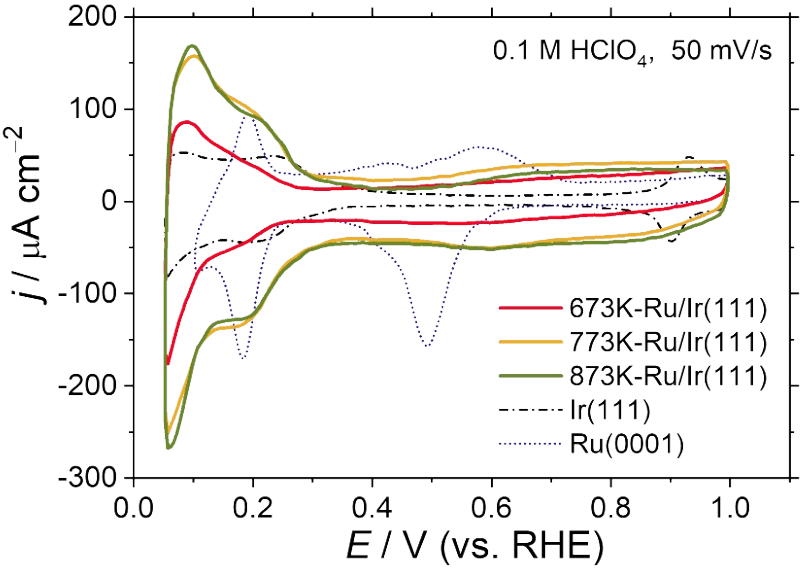

Figure S.4 CV curves in N_2-purged 0.1 M $HClO_4$

Cyclic voltammetry (CV) was conducted in an N_2-purged glove box immediately after the sample transfer. A conventional three-electrode cell (not the SECM cell) was used, and a reversible hydrogen electrode (RHE) and Pt wire were employed as the reference electrode and counter electrode, respectively. The surface area of the sample working electrodes was determined by an O-ring (0.09 cm^2, Kalrez, DuPont). CV curves were obtained in N_2-purged 0.1 M $HClO_4$, and the scan rate was 50 mV/s.

The CV curves of the samples are shown in Figure S.4, accompanied by the curves for vacuum-cleaned Ir(111) and Ru(0001). The reference CV characteristics of clean Ir(111) (dash-dotted)[2–4] and Ru(0001) (dotted)[4–6] are in good agreement with previous reports.

Below 0.4 V, *x* K-Ru/Ir(111) showed redox peaks with a shoulder, although the feature was weak and obscure for 673 K-Ru/Ir(111). In general, redox features on CV curves in low potential regions correlate with hydrogen adsorption/desorption behaviours, but the adsorption of O/OH species can be realised in these low potential regions (< 0.4 V) on Ir(111)[2,4] and Ru(0001)[4–6] due to their high oxygen affinity.[7] Therefore, both hydrogen and O/OH adsorption and desorption should be considered for the redox peaks of Ru/Ir(111) below 0.4 V in CVs recorded using the conventional three-electrode cell in N_2-purged 0.1 M $HClO_4$. This assignment can be rationalised, cross-referencing with the HOR deactivation behaviour above the certain potential (Figure 3 (a)), where surface O/OH species would act as active site blockers. In addition, an increase in double layer charges (ca. 0.4–0.8 V) as well as a disappearance of the redox feature at ca. 0.9 V were observed for the *x* K-Ru/Ir(111) contrary to that

on clean Ir(111). Although no attempt has been made to clarify the detailed assignments for the CV peaks of Ir-Ru bimetallic surfaces in such relatively high potential region (> 0.4 V), similar result was reported for the voltammograms of Pt(111) modified with atomic height Ru island recorded in 0.1 M $HClO_4$, in which the double layer charge increased by the modification.[8,9]

E. Mathematical Estimation of the Ensemble Probability

The calculation of the dimer site probability was reported previously.[10] First, randomly distributed Ir and Ru atoms with the closest packed structure (i.e. (111) of a face-centered-cubic (FCC) or (0001) of hexagonal-close-packed (HCP) crystal structures) are assumed. When the atomic arrangement comprising seven atoms (close-packed unit) is considered as a unit structure, the arrangement of atoms can be separated into 14 groups (A, B, C… N) considering the dimer site ratio (Figure S.5). Because each group has various patterns (Figure S.7), the number of patterns must be multiplied to calculate the probabilities for each dimer. Therefore, the probability of XX (Ir_2, Ru_2, or IrRu) at a given surface Ru composition of x_{Ru} ($0 < x_{Ru} < 1$) can be calculated using the following equations:

$$\frac{C_{XX}(x_{Ru})}{C_{Ir_2}(x_{Ru}) + C_{Ru_2}(x_{Ru}) + C_{IrRu}(x_{Ru})} \#(S.1)$$

where

$$C_{XX}(x_{Ru}) = \sum_{Group\ A\ to\ N} \left(\frac{1}{x_{Ru}}\right)^{n} \left(\frac{1}{1 - x_{Ru}}\right)^{7-n} \times r_{XX} \times (Number\ of\ patterns) \#(S.2)$$

and n and $7–n$ (exponentiation) are the number of Ru and Ir atoms in the group, respectively. r_{XX} represents the ratio of XX. The values summarized in Table S.1 were used for these calculations. The probability of trimers can also be estimated in the same manner even though the group must be divided into 22 groups, as shown in Table S.2. Note that the stacking relationship to the 2nd layer of FCC stacking (i.e. whether the centre of the trimers is FCC hollow or HCP hollow) is not distinguished.

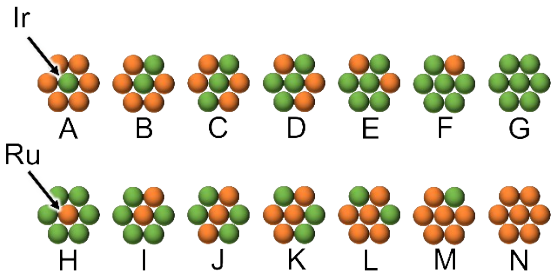

Figure S.5 Figure 6 Representative atomic arrangement patterns of groups A to N. Groups A to G (H to L) have an Ir (Ru) atom at centre position, and number of nearest neighbouring Ru (Ir) atoms surrounding the centre atom determine the groups.

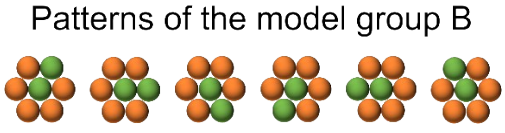

Figure S.7 Six patterns (atomic arrangements) of group B are displayed as an example.

Table S.1 List of dimer ratio, number of atoms, and number of patterns for each group

Group	*r* (Dimer ratio)			*n* (Ru)	7–*n* (Ir)	Number of patterns
	Ir_2	Ru_2	IrRu			
A	0	0	1	6	1	1
B	1/6	0	5/6	5	2	6
C	1/3	0	2/3	4	3	15
D	1/2	0	1/2	3	4	20
E	2/3	0	1/3	2	5	15
F	5/6	0	1/6	1	6	6
G	1	0	0	0	7	1
H	0	0	1	1	6	1
I	0	1/6	5/6	2	5	6
J	0	1/3	2/3	3	4	15
K	0	1/2	1/2	4	3	20
L	0	2/3	1/3	5	2	15
M	0	5/6	1/6	6	1	6
N	0	1	0	7	0	1

Table S.2 List of trimer ratio, number of atoms, and number of patterns for each group

Group	*r* (Trimer ratio)				*n* (Ru)	7–*n* (Ir)	Number of patterns
	Ir_3	Ir_2Ru	$IrRu_2$	Ru_3			
A	0	0	1	0	6	1	1
B	0	1/3	2/3	0	5	2	6
C1	1/6	1/3	1/2	0	4	3	6
C2	0	2/3	1/3	0	4	3	9
D1	1/3	1/3	1/3	0	3	4	6
D2	1/6	2/3	1/6	0	3	4	12
D3	0	1	0	0	3	4	2
E1	1/2	1/3	1/6	0	2	5	6
E2	1/3	2/3	0	0	2	5	9
F	2/3	1/3	0	0	1	6	6
G	1	0	0	0	0	7	1
H	0	1	0	0	1	6	1
I	0	2/3	1/3	0	2	5	6
J1	0	1/2	1/3	1/6	3	4	6
J2	0	1/3	2/3	0	3	4	9
K1	0	1/3	1/3	1/3	4	3	6
K2	0	1/6	2/3	1/6	4	3	12
K3	0	0	1	0	4	3	2
L1	0	1/6	1/3	1/2	5	2	6
L2	0	0	2/3	1/3	5	2	9
M	0	0	1/3	2/3	6	1	6
N	0	0	0	1	7	0	1

F. Comparison of Calculated Dimer (a) and Trimer (b) Sites and SECM-estimated HOR Standard Rate Constants (k^0) vs. Surface Ru Composition of *x* K-Ru/Ir(111)

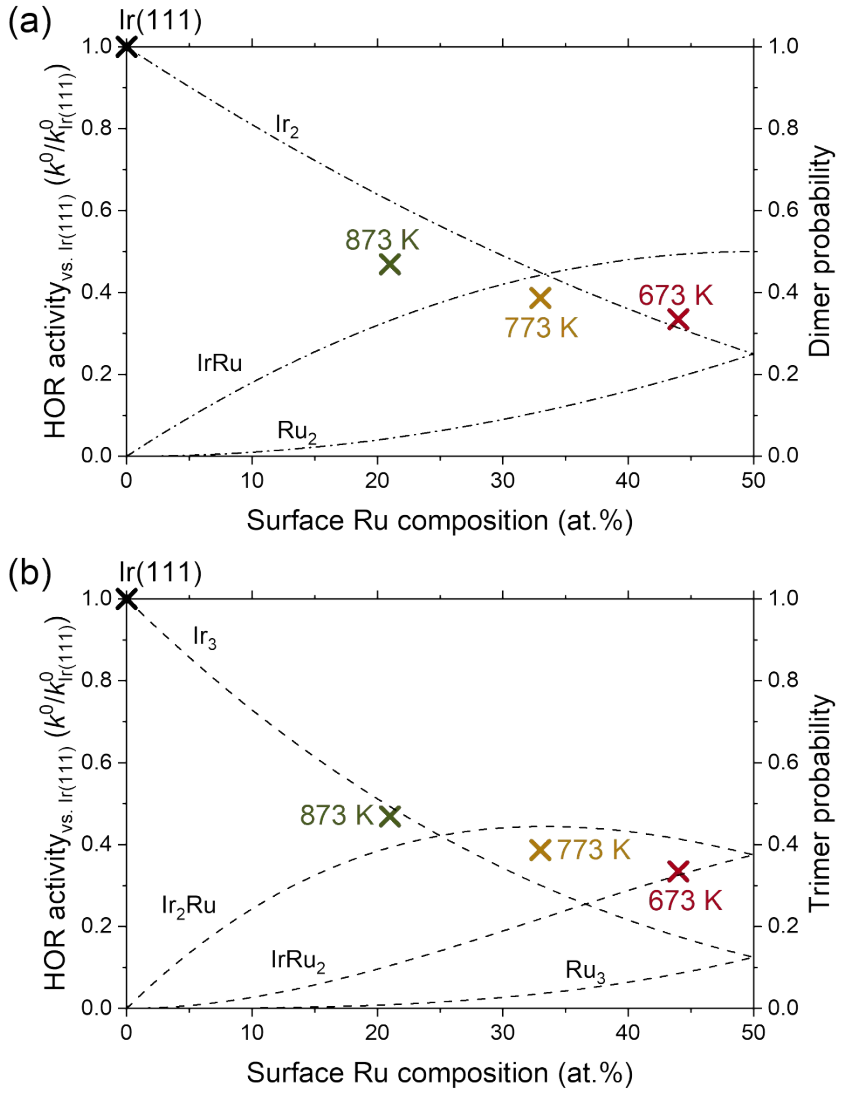

Figure S.8 SECM-estimated HOR activity for *x* K-Ru/Ir(111) (k^0) normalized by that of clean Ir(111) ($k^0_{Ir(111)}$) vs. LE-ISS estimated surface Ru compositions. The surface-Ru-composition-dependent mathematically calculated probability of various dimers (a) and trimers (b) are also shown as dash-dotted and dashed lines, respectively.

The SCEM-estimated HOR activity trends (k^0) vs. surface Ru atomic compositions fit better with pure Ir (Ir_2 and/or Ir_3) sites than the other Ru-containing sites.

References

1. H. Okamoto, *J. Phase Equilibria*, **13**, 565–567 (1992).

2. J. Wei et al., *Electrochim. Acta*, **246**, 329–337 (2017).

3. R. Gómez and M. J. Weaver, *Langmuir*, **18**, 4426–4432 (2002).

4. M. T. M. Koper, *Electrochim. Acta*, **56**, 10645–10651 (2011).

5. A. M. El-Aziz and L. A. Kibler, *Electrochem. commun.*, **4**, 866–870 (2002).

6. M. P. Mercer and H. E. Hoster, *Electrocatalysis*, **8**, 518–529 (2017).

7. J. K. Nørskov et al., *J. Phys. Chem. B*, **108**, 17886–17892 (2004).

8. W. F. Lin et al., *J. Phys. Chem. B*, **103**, 6968–6977 (1999).

9. T. Iwasita, H. Hoster, A. John-Anacker, W. F. Lin, and W. Vielstich, *Langmuir*, **16**, 522–529 (2000).

10. K. Ishikawa, J. Ohyama, K. Okubo, K. Murata, and A. Satsuma, *ACS Appl. Mater. Interfaces*, **12**, 22771–22777 (2020).